Composites Part C: Open Access 17 (2025) 100568

Contents lists available at ScienceDirect

Composites Part C: Open Access

journal homepage: www.sciencedirect.com/journal/composites-part-c-open-access

A novel and rapid method of integrating sensors for SHM to thermoplastic composites through induction heating

Tasdeeq Sofi [a,b,*], Javier A. García [a], María R. Gude [a], Peter Wierach [b,c]

[a] Foundation for the Research, Development and Application of Composite Materials (FIDAMC), Avda. Rita Levi Montalcini 29, Tecnogetafe, 28906, Getafe, Spain
[b] Institut für Polymerwerkstoffe und Kunststofftechnik TU Clausthal, Agricolastraße 6, 38678, Clausthal-Zellerfeld, Germany
[c] German Aerospace Center (DLR), Lilienthalplatz 7, 38108, Braunschweig, Germany

ARTICLE INFO

Keywords:
Piezoceramic transducers
Thermoplastic adhesive films
Induction heating
Thermoplastic composites
Mechanical testing
SHM

ABSTRACT

A novel, rapid, and efficient method for bonding Piezoceramic transducers (PCTs) to high-performance thermoplastic composites using thermoplastic adhesive films (TPAFs) and induction heating is presented. The current state-of-the-art techniques to bond PCTs to composites using epoxy adhesives can take hours. This innovative out-of-oven or autoclave procedure drastically reduces bonding time to mere minutes, thereby significantly enhancing the process efficiency. Five different TPAFs were used to bond PCTs to carbon fiber polyether-ether-ketone (CF-PEEK) coupons. After determining the process window and analyzing the effects of power, coupling distance, and time on temperature, it was found that power has the greatest influence. A 20% increase in power can result in 50.9% increase in temperature as compared to time. Controlled heating and cooling ramps were developed based on the power-temperature correlation, and their effects were analyzed through differential scanning calorimetry tests. In the controlled case, the melting enthalpy of semi-crystalline TPAF increased by 4.2%, while the glass transition temperature of amorphous TPAF increased by 2.4% compared to non-controlled case. Following successful PCT bonding, mechanical performance was evaluated through static flexural and fatigue tests. TPAFs exhibited critical strains of 0.33%-0.71%, with some exceeding the critical strains of co-bonded or epoxy-bonded PCTs in previous studies by 0.13%. Microscopic analyses revealed the dominant failure mode at the composite-adhesive interface. During fatigue testing, three out of five TPAFs performed successfully, with the highest change in electro-mechanical susceptance spectra observed in amorphous TPAF equivalent to 1.87%. Overall, an efficient methodology is proposed, particularly beneficial for applications in structural health monitoring.

List of abbreviations

Abbreviation	Full Form
CFRP	Carbon Fiber Reinforced Plastic
BVID	Barely Visible Impact Damage
NDI	Non-Destructive Inspection
CBM	Condition-Based Maintenance
SHM	Structural Health Monitoring
PCT	Piezoceramic Transducers
GW	Guided Wave
TP	Thermoplastic
PEEK	Poly-Ether-Ether-Ketone
TPC	Thermoplastic Composite
TPAF	Thermoplastic Adhesive Film
IH	Induction Heating
AUCT	Acousto-Ultrasonic Composite Transducers
DSC	Differential Scanning Calorimetry
TPF	Thermoplastic Film
C_d	Coupling Distance
HR	Heating Rate
CR	Cooling Rate
T_m	Melting Temperature
T_g	Glass Transition Temperature
CS	Critical Strain
EMS	Electro-Mechanical Susceptance
RMSD	Root Mean Square Deviation

* Corresponding author.
E-mail address: sofi.tasdeeq@fidamc.es (T. Sofi).

https://doi.org/10.1016/j.jcomc.2025.100568

Available online 6 February 2025

1. Introduction

Despite the excellent performance and growing demand for carbon fiber reinforced plastic (CFRP) composites do not have an exceptional impact resistance. During operation and maintenance, CFRP composites are susceptible to various forms of damage, including impact, fatigue, and environmental degradation. Compliance with industry regulations concerning safety along with the challenging detection of damages, particularly barely visible impact damages and the complexity of accurately predicting fracture mechanics in composites, thorough non-destructive inspections (NDI) are conducted on such structures periodically. The NDI maintenance approach, driven by predetermined schedules, incurs significant costs and renders the assets unavailable during the inspection period [1]. To overcome the drawbacks faced in the case of scheduled maintenance, a new maintenance strategy known as condition-based maintenance (CBM) is gaining attention. In CBM, maintenance timing is ascertained through the continuous monitoring of the asset, a practice referred to as structural health monitoring (SHM). SHM is defined as the systematic process of gathering and analyzing data obtained from a distributed network of sensors bonded to or embedded within a structure to obtain information about the health of the structure [2,3].

One of the promising technologies that can be used for SHM is piezoceramic transducers (PCTs) based guided wave (GW) SHM. It has emerged as a relatively mature technology and is being widely used for SHM of composite structures [2,4]. However, there are still many challenges to bring this technology to maturity for its widespread use to monitor real structures. One such challenge where research is needed is the easy, fast, and cost-efficient integration of PCTs with the composite structure, as pointed out in a report [5] by the Sandia National Labs involving different stakeholders within the aeronautical sector, including original equipment manufacturers, owners, and operators. Approximately 63% of the participants acknowledged the need for research focused on integrating SHM systems with the structures, while about 50% emphasized the significance of researching SHM electronics, with a focus on aspects such as size, weight, cost, durability, and reliability, among others. This viewpoint remains valid given the current state-of-the-art, where integrating PCTs with the composite structures involves secondary bonding using epoxy adhesives, primarily through manual methods. This approach results in challenging repair procedures for malfunctioning PCTs and an overall process that is not cost-effective and demands considerable time and labor.

The integration of sensors with composite structures primarily follows two strategies, namely secondary bonding and co-bonding [6]. Secondary bonding entails bonding PCTs to the surface of the composite host structure in a separate step after manufacturing the part. It is a reliable and extensively used method for PCT installation. However, it adds an extra step, resulting in higher installation costs. On the other hand, in co-bonding, PCTs are placed either on the surface or embedded within the uncured composite structure. Co-bonding significantly reduces the sensor installation time; however, this process exposes the sensors to elevated pressure and temperature levels, typical of procedures like autoclave curing which can lead to pre-stresses in them. The integration of PCTs with high-performance thermoplastic (TP) carbon fiber (CF) composites, such as polyether-ether-ketone, is more challenging in comparison to thermoset-based composites. Co-bonding PCTs to these types of composites is either extremely difficult or in some cases, unachievable. This is primarily due to the potential damage of the PCT, which can occur from the elevated temperatures and shear forces induced by the high viscosity of these polymers. Conversely, secondary bonding also poses difficulties because of the low surface energy exhibited by such polymers. TP composite (TPC) structures have garnered increased attention in the aeronautical industry [7]. Consequently, there exists a pressing need to devise efficient and cost-effective solutions for the integration of sensors with TPC structures.

One such approach involves the utilization of TP adhesive films (TPAFs) instead of epoxy adhesives, offering distinct advantages such as indefinite shelf life, simplified reparability, easier processing, and suitability for room-temperature storage. In a previous study [8], PCTs were bonded to CF PEEK (CF-PEEK) composite specimens by TPAFs through oven vacuum bagging. The subsequent evaluation of these bonded PCTs under standard aeronautical operational environmental conditions demonstrated better performance when compared to an epoxy adhesive film. However, the conventional method of heating TPAFs in an oven is costly, requires long heating cycles, requires significant consumable usage, and the need to put the entire structure in the oven can prove expensive and cause potential thermal degradation of the structure. To address these limitations, this study proposes a novel, more efficient, and rapid bonding technique. The basic concept involves providing the necessary heat for melting the TPAF through the Joule effect, achieved by applying an induction field to the CF composite, as opposed to relying on an oven or alternative heating methods. This bonding approach proves cost-effective, easier, and significantly faster, reducing bonding time from hours to just a few minutes compared to epoxy or TPAF bonding conducted in an oven or using heat blankets. Moreover, it minimizes consumable usage and applies heat locally, thus mitigating the adverse effects of thermal degradation on the structure.

Induction heating (IH) is primarily used in composite applications for welding of TPC parts due to their ability to be remelted and reformed [9–12]. In this study, the aim is to use heat generated by IH to melt TPAFs for bonding PCTs. In literature, only a few studies that used IH to bond sensors to metallic parts. For instance, in [13], micro-electromechanical system-based strain sensors were bonded to steel through IH, achieved by inserting a tin-silver eutectic solder layer between the sensor and the steel surface. The study showed that the sensors can be bonded in a few seconds with very good bond properties. In [14], silicon chips were bonded to different metallic surfaces such as silver, copper, etc. using IH. Similarly, in [15], semiconductor components were bonded to direct bonded copper using a silver-sintering paste layer in a relatively short time. The bonding of high-temperature sensors using a TPAF to metallic surfaces has been proposed in a patent by Lu et al. [16]. The invention describes methods of using TPAFs as bonding layers for bonding high-temperature sensors to metallic structures. In all of these studies or inventions mentioned above, the bonding of the sensors or electronic components was carried on metallic surfaces. However, challenges arise when bonding sensors to TPCs. Firstly, metals are good conductors of electricity, and consequently IH is particularly effective with them. However, this is not the case with TPCs as they are not good conductors. Therefore, achieving a certain temperature and controlling it to properly melt the TPAFs for bonding is relatively difficult. Secondly, the choice of the adhesive film used for bonding is more restricted in the case of TPCs because of the temperature limit, which is generally higher in case of metals used for aircraft. Thirdly, sensor bonding with metals is relatively easier because of their higher surface energy. Whereas, bonding sensors to TPCs presents distinct challenges due to their lower surface energy exhibited by these materials.

Table 1
TPAFs used to bond the AUCTs [8].

TPAF	Material	Supplier	Molecular structure	Average SLS [MPa]
P22100 (TPF1)	Polyolefin (POF)	Pontacol	Semi-crystalline	4.22 ±0.31
P22110 (TPF2)	Low-density polyethylene			3.95 ±0.32
P45200 (TPF3)	POF/Copolyamide (Multi-layer)			4.80 ±0.56
P22400 (TPF4)	High-density polyethylene			4.48 ±0.26
T-Link (TPF5)	Epoxy TP	L&L products	Amorphous	9.20 ± 0.71

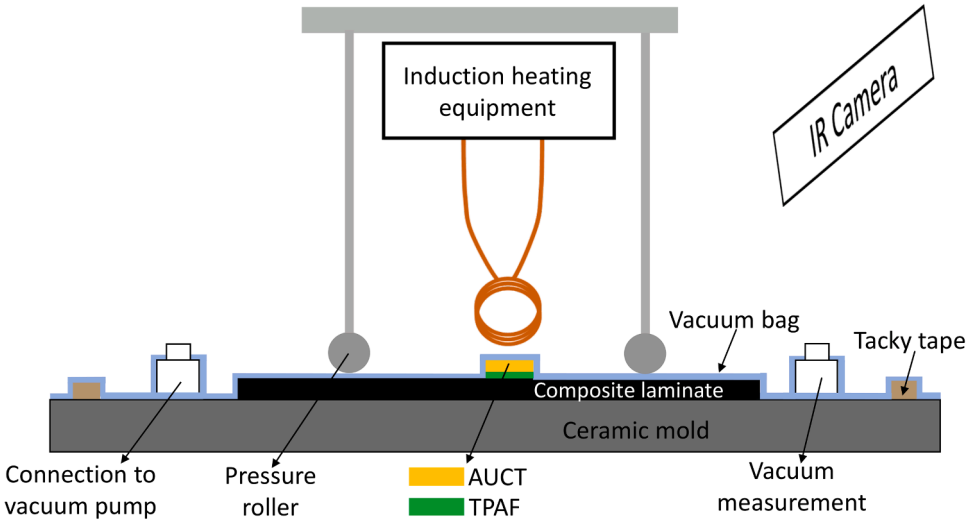

Fig. 1. Induction heating setup for bonding the AUCTs to a composite structure.

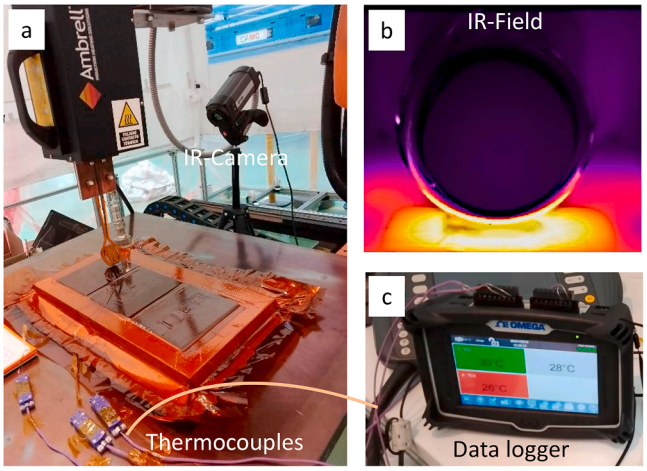

Fig. 2. Setup for monitoring temperature during induction heating: (a) IR-camera and IH setup, (b) recorded IR-field and, (c) data logger for measuring temperature with thermocouples.

Table 2
Process study parameter levels.

Study	Power [Amp]	Coupling distance [mm]	Time [s]
Process window determination	120, 130, 140, 150	3, 5, 7	25, 30, 35, 40
Sensitivity analysis	78, 130, 182	3, 5, 7	18, 30, 42

A few previous studies [8,17] have demonstrated the usage of TPAFs to bond sensors to composite surfaces, however the TPAFs were either melted in an oven or heat blankets, offering easier process control compared to IH. However, these methods are inefficient in terms of cost and labor. To the best of knowledge of the authors there is a lack of existing studies concerning the bonding of transducers or sensors to composite structures utilizing IH. This is the first study demonstrating the application of IH to bond transducers and sensors to composite parts. The objectives of this study are:

- Investigating a rapid bonding method for PCTs to high-performance TP parts using TPAFs.
- Studying and developing a controlled process for processing TPAFs.

Table 3
Thermal analysis cases with different heating and cooling rates.

Case	Heating rate [°C/min]	Cooling rate [°C/min]	Isothermal condition maintained at T_m for 2-3 minutes?
Case 1A	200	43	No
Case 1B	200	43	Yes
Case 2	11	43	No
Case 3A	200	12	No
Case 3B	200	12	Yes

- Exploring the influence of heating and cooling phases on the TPAF properties.
- Evaluating the mechanical performance of PCTs bonded with IH through static and cyclic mechanical tests.

2. Materials and methods

2.1. Materials

The test specimens were prepared with CF-PEEK composite material. Two different types of CF reinforcement, commonly employed in the aeronautical industry, were used in this study. These reinforcement materials were the APC2-AS4 unidirectional CF-PEEK tape supplied by Solvay, and the HTA-40 woven CF-PEEK prepreg supplied by Tejin™. The APC2-AS4 coupons were manufactured through oven vacuum bagging, while the HTA-40 coupons were fabricated utilizing a hot-press. Following which the PCTs were bonded onto these coupons.

The PCTs were supplied from PI Ceramic®, Lederhose, Germany. These are special PCTs embedded in a ductile polymer and provided with a mechanical precompression to form an "acoustic-ultrasonic composite transducer (AUCT)" [18]. The selection of the TPAFs for bonding the AUCTs to TPC was governed by specific criteria. Primarily, their melting temperature (T_m) needed to be below 150 °C to align with the temperature limitation of the AUCTs. Additionally, these TPAFs were required to have a deflection temperature exceeding 70 °C to comply with aeronautical environmental condition standards (DO-160) while also ensuring good bonding strength. Thermal and mechanical tests namely differential scanning calorimetry (DSC) test and single lap shear tests were conducted to ensure that the TPAFs meet the set criteria

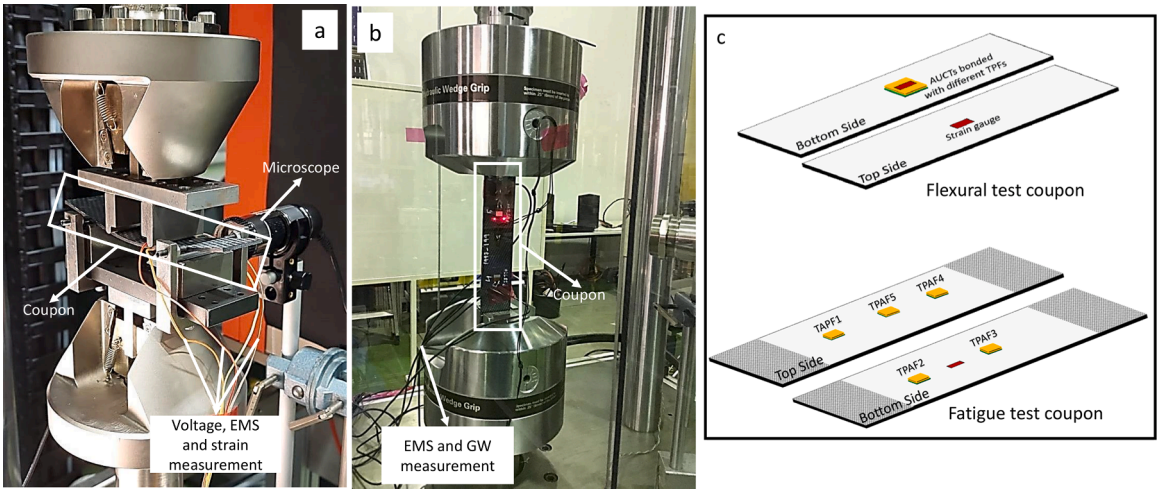

Fig. 3. Mechanical tests (a) Four-point quasi-static flexural test setup, (b) Tensile-Tensile fatigue test setup and, (c) Flexural test coupon (top) and fatigue test coupon (bottom).

Table 4
Material and test specifications of flexural and fatigue tests.

Material and testing specifications	Flexural test	Fatigue test
Material and coupon dimensions	• CF-PEEK composite woven HTA-40 with dimensions 150*30*2.17 mm^3. • CF-PEEK composite unidirectional APC2-AS4. 150*30*2.16 mm^3.	CF-PEEK composite woven HTA-40 with dimensions 300*55*2.17 mm^3.
Adhesive used	TPF3, TPF4, TPF5 and two-part epoxy adhesive namely Loctite EA-9466, layout Fig. 3(c)top.	Five TPAFs (Table 1), layout Fig. 3(c) bottom.
Strain ramp (flexural test) or Number of fatigue cycles (fatigue test)	0.1% strain and incrementing in 0.1% steps up to 0.8%.	200k cycles at a frequency of 10 Hz and r-ratio of 0.1, with the maximum load applied was 10 kN.
Measurements	• Strain on the coupon and AUCT • EMS spectra after every 0.1% strain ramp with C60 impedance analyzer from Cypher instruments over a range of 1 kHz to 1 MHz with a resolution of 1000 Hz.	• EMS spectra after specific number of cycles. • GW measurements after a specific number of cycles with each AUCT acting as a transducer in a sequential manner, while other AUCTs functioned as sensors.

[8]. Five different TP films (TPF) meeting the criteria were identified and are shown in Table 1.

2.2. Bonding by induction heating

The fundamental principle underlying the IH bonding process involves the generation of heat through the Joule effect when an inductive field is applied to a conductive material. To achieve this, a TPAF is positioned between the host composite and the AUCT, maintaining pressure through vacuum bagging. Following this, a local induction field is applied specifically at the AUCT location. Given the conductivity nature of the carbon fiber, heat is generated through the Joule effect. This resultant heat melts the TPAF through conduction, establishing a bond between the composite part and the AUCT upon cooling. An Ambrell EasyHeat IH system, equipped with a solenoid-shaped coil operating at a coil frequency of 240–280 kHz, was employed to generate the induction field. Fig. 1 shows the schematic of the complete setup for bonding the AUCT using the IH method.

2.3. Process study and control

A detailed investigation was conducted to determine the required process parameters essential for achieving proper melting of the TPAFs. This included determining the proper process window, an analysis of the influence of different process parameters on the generated temperature, and the development of a controlled cycle for processing the TPAFs. The temperature was recorded at the center of the AUCT bonding region on a CF-PEEK (HTA-40) composite coupon with dimensions of 80 × 80 × 2.17 mm^3 with an E-type thermocouple and data logger provided by Omega™, at a sampling rate of 10 samples/sec. Additionally, an IR camera from FLIR was employed to capture the temperature field within the bonding and adjacent areas shown in Fig. 2. In an IH process, the three primary process parameters are the supplied power to the coil, the coupling distance (C_d) which is the distance between the coil and the host structure, and the duration for which the field is applied. The process window determination involved a study of power at four different levels, coupling distance at three levels, and time across four levels, as shown in Table 2.

Following the establishment of the suitable process conditions, a sensitivity analysis was performed by investigating the impact of individual process parameters across three different levels using a full-factorial design and three repetitions for each experiment, outlined in Table 2. The objective was to understand the influence of individual parameters on the generated temperature and identify the most influential factor. This understanding would be important for implementing an effective heating ramp for the TPAF, enabling control over both the heating and cooling phases. The heating and cooling phases of the TPAF can be applied in three distinct manners. In the first approach, an induction field is applied using predetermined process parameters, concluding the heating ramp around the T_m of the TPAF, followed by natural cooling to room temperature. This procedure results in a very high heating rate (HR) and cooling rate (CR). In the second approach, a slower HR is utilized to ensure that the maximum temperature generated reaches a saturation point around the T_m of the TPAF. The process parameters, such as power or C_d, are carefully chosen to ensure the temperature saturates around the T_m of the TPAF, irrespective of the duration the induction field is applied. Consequently, this method yields a slower HR, ensuring proper TPAF melting before transitioning to the cooling phase. In both these approaches, the CR remains high,

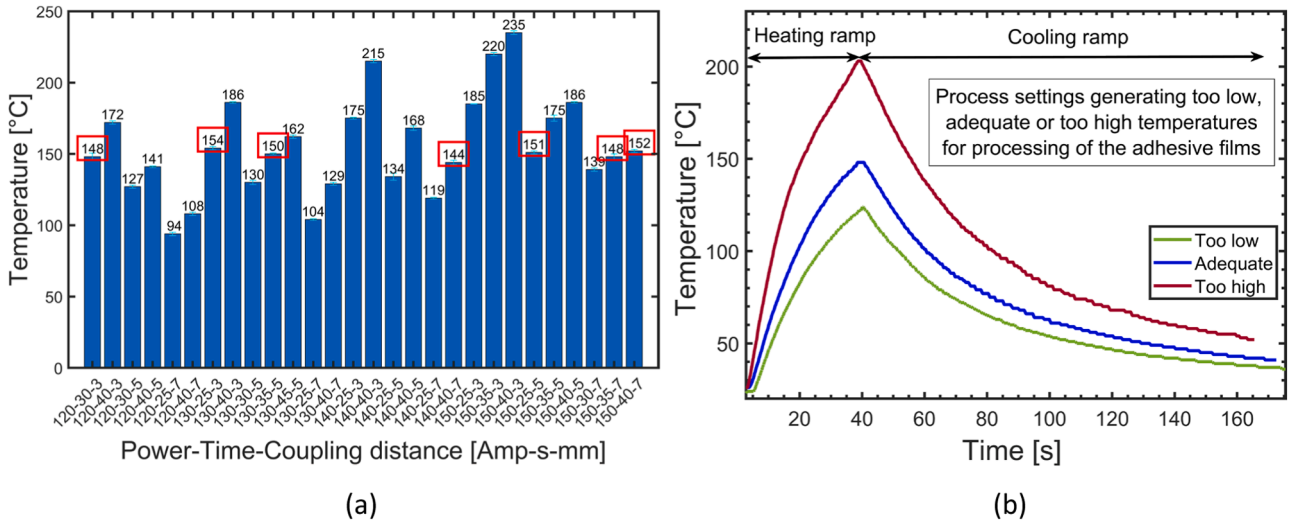

Fig. 4. Process study (a) Temperatures generated for different process parameter combinations and (b) Temperatures profile for three different process parameter settings.

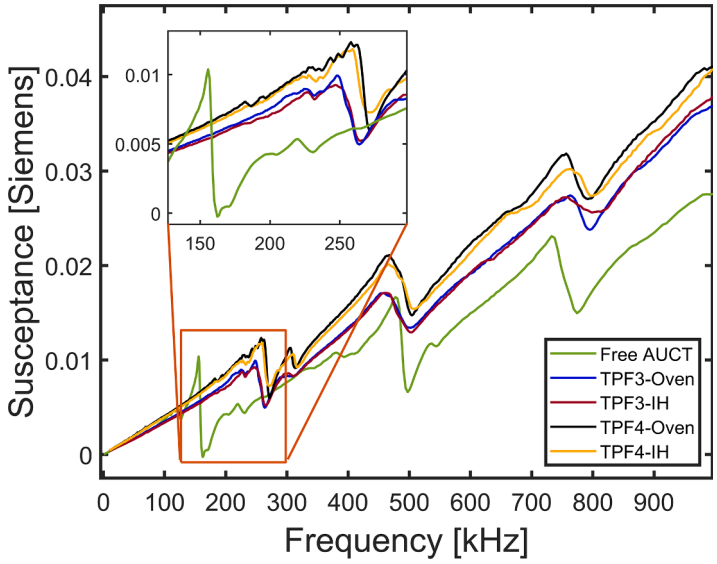

Fig. 5. EMS spectra for TPF3 and TPF4 with oven and induction heating processed as well for a free AUCT.

potentially impacting the crystallinity of the TPAF and therefore the mechanical properties of the adhesive bond [19]. A third method was developed to better control the CR as well. In this third approach, predetermined process parameters are used to rapidly reach the T_m. Subsequently, by dynamically adjusting these parameters, the T_m is maintained for a brief duration, followed by gradual cooling of the TPAF to its T_g. This controlled cooling process aims to enhance the crystallinity of the semi-crystalline TPAFs to achieve better mechanical properties of the adhesive bond.

2.4. Thermal analysis

Two primary distinctions arise when comparing the heating of TPAFs using an oven versus IH. Firstly, the melting of TPAFs in an oven predominantly occurs through convection, while in IH, it primarily occurs through conduction. Secondly, the rate of heating and cooling in an oven is considerably slower compared to IH. Although the HR is not a critical factor, the CR holds significance due to its impact on crystallinity and, consequently, the mechanical properties of the adhesive bond. As discussed in the preceding section, three different methods can be employed to melt and cool the TPAFs with varying HR and CR ramps. To simulate these three methods, five distinct test cases were examined through a DSC test as described in Table 3. Cases 1A and 1B, Case 2 and Cases 3A and 3B represent the first, second, and third method respectively. The DSC tests were conducted using a DSC Q200 TA Instruments apparatus in accordance with the ISO 11,357–3 standard. Two different TPAFs, representing both semi-crystalline (TPF4) and amorphous (TPF5) polymer structures, were subjected to these tests. In the DSC tests, the heating and cooling ramps applied during IH were replicated in the first cycle. Subsequently, a second cycle followed, adhering to the mentioned standard heating and cooling ramps (heating from 30 °C to 180 °C at 20 °C/min and cooling to 30 °C at 20 °C/min). The objective was to measure the T_m and melting enthalpy or T_g in the standard heating ramp to evaluate the influence of these different cases on the performance of the TPAFs.

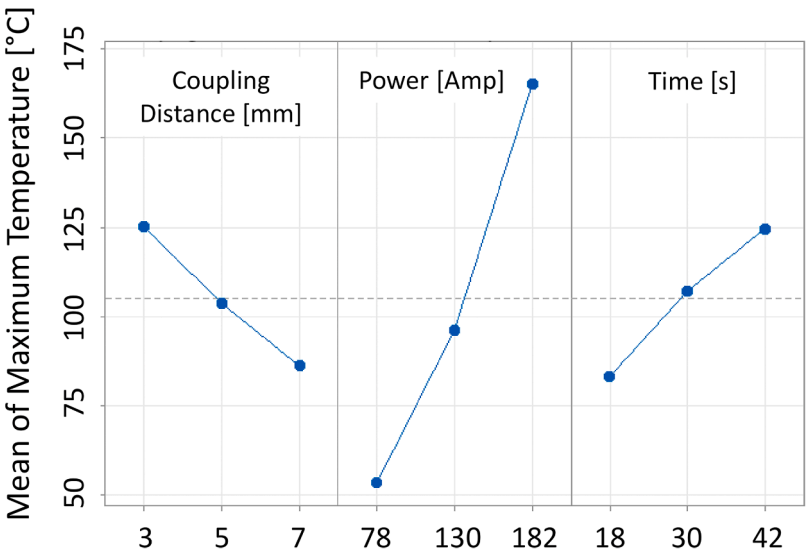

Fig. 6. Maximum temperature generated as a function of coupling distance, power, and time.

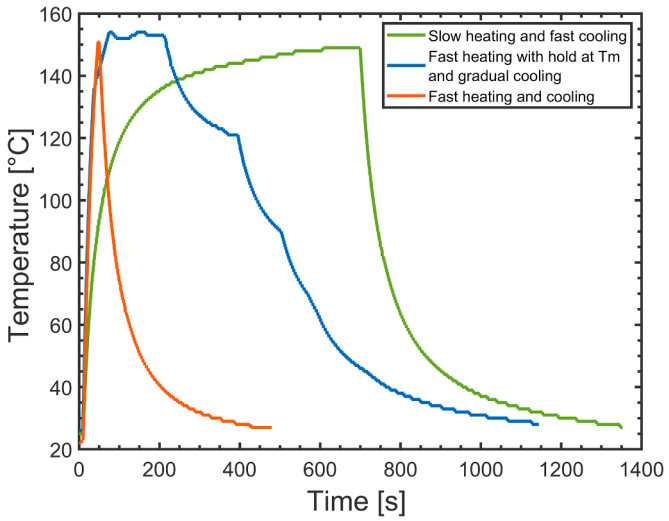

Fig. 7. Heating and cooling ramps for different processing methods for TPAFs.

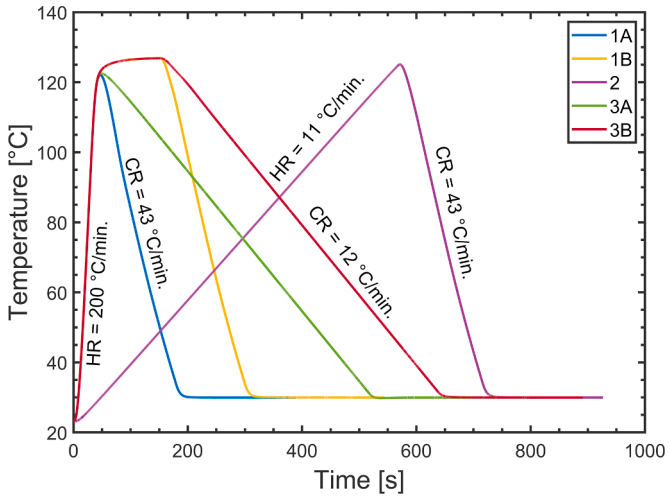

Fig. 8. Thermal analysis cases with different heating and cooling rates for processing of TPAFs.

2.5. *Mechanical testing*

Mechanical tests were conducted to investigate the performance of the AUCTs bonded using IH in static and cyclic loading. A four-point quasi-static flexural test setup was to characterize the strain at which the transducer fails, known as the critical strain (CS). The test setup is depicted in Fig. 3(a) and the material and test specifications are given in Table 4. A minimum of three samples were tested for each adhesive. Strain gauges (3/120 LY11), supplied by HBM, Germany, were used to measure the strain with a sampling rate of 10 samples/*sec* on the coupon (serving as the control strain) and the transducer. During the loading and unloading ramps, strain was measured with a sampling rate of 10 Hz and the generated voltage was monitored and recorded using an Oscilloscope namely PicoScope® 4000A from Pico technology at a sampling rate of 20 div/s. Substantial alterations in strain and voltage values indicate AUCT failure [20]. The electro-mechanical susceptance (EMS) which is the imaginary part of the electro-mechanical admittance, is a well-known indicator of the health and bonding condition of an AUCT [17,20–22] that can be used to determine the CS of an AUCT. A microscope placed behind the test setup allowed for capturing images after each ramp to detect if any cracks developed in the AUCT. The CS of the AUCT was determined by combining the results from all the aforementioned measurements and observations. Additionally, post-testing, a microscopic analysis was conducted on a few tested coupons to observe any cracks in the adhesive bond layer and/or on the AUCT during the flexural tests, revealing the various failure modes. For comparison microscopic analysis was carried on a few untested coupons as well. The flexural tests were conducted for both AUCTs bonded with controlled and uncontrolled cooling ramps.

A preliminary study was conducted to evaluate the long-term functional performance of the AUCTs through fatigue testing under tensile-tensile loading conditions. The tensile-tensile fatigue test was selected because the coupon specimen represents a segment of an aircraft fuselage structure, where cyclic tensile stresses play a significant role. This test simulates the repetitive tensile forces experienced during pressurization cycles and operational conditions. These fatigue tests were conducted on a 100 kN Zwick universal testing machine as shown in Fig. 3 (b) and the material and test specifications are given in Table 4. The AUCTs bonded with TPF1 to TPF5 will be denoted by S1 to S5 respectively. The GWs were actuated and received using a National

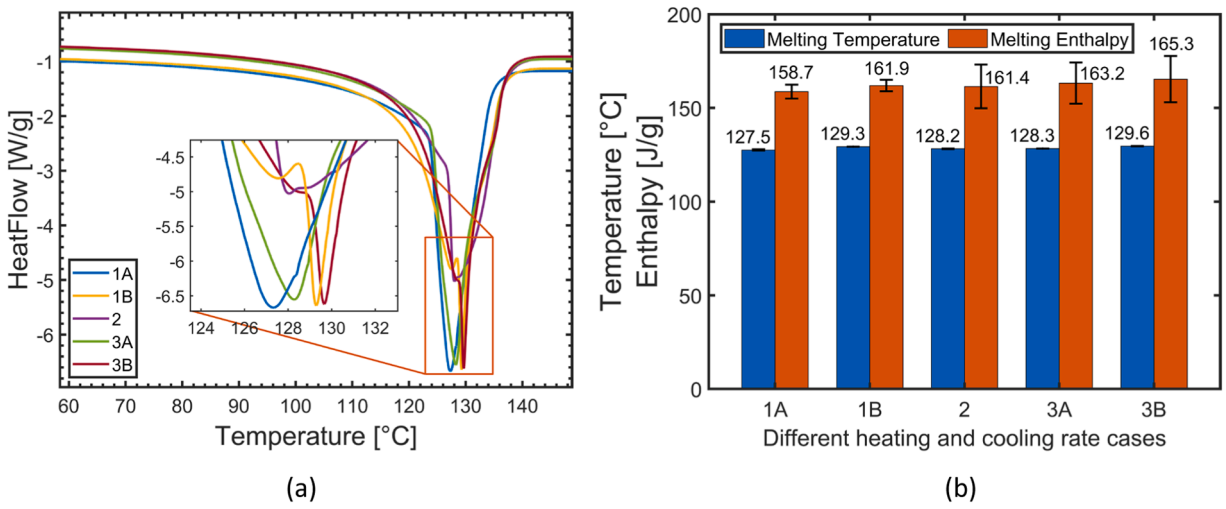

Fig. 9. Thermal analysis cases for TPF4 (a) DSC curves and (b) Melting temperatures and enthalpies.

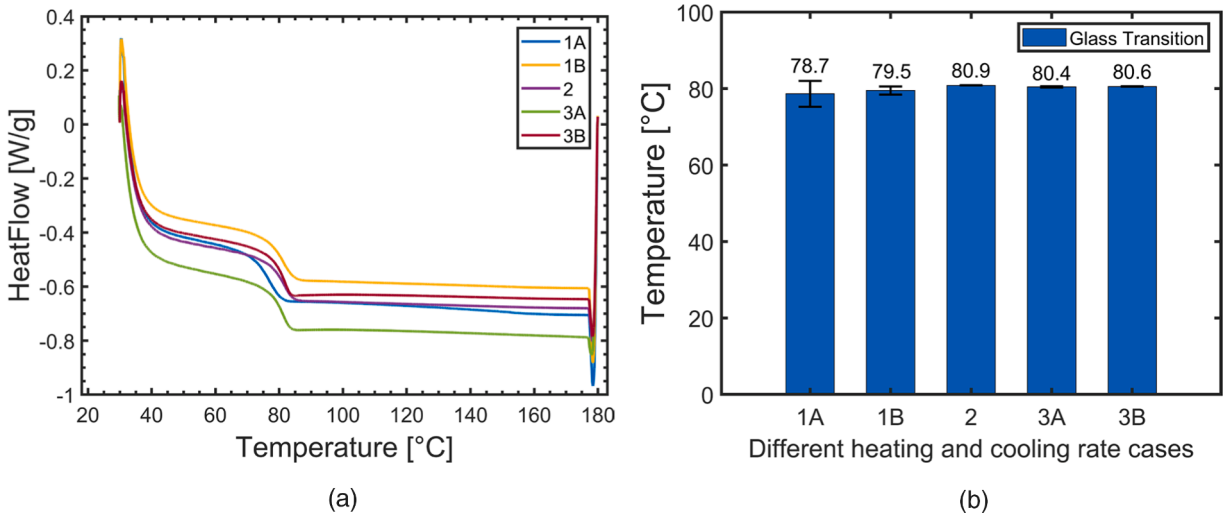

Fig. 10. Thermal analysis cases for TPF5 (a) DSC curves and (b) Glass transition temperatures.

Instruments PXIe-1082. A three-pulse sine wave, employing a Hanning window and having an amplitude of 3 Volts, was used as the actuation signal. The frequency sweep spanned from 40 kHz to 350 kHz, with intervals of 10 kHz. Each signal underwent ten recordings, which were subsequently averaged, and the measurements were conducted over a 600 μs duration. To determine AUCT damage or debonding, the GW signals acquired after a certain number of fatigue cycles were compared against the baseline (first measurement) at two distinct frequencies: 50 kHz and 250 kHz which represent a low and high frequency case where two fundamental modes namely A0 and S0 generally emerge for similar material, layup and thickness [23–25]. For this comparison, only the first segment of the signal was taken into account. This particular segment holds significance in the context of damage detection and aids in mitigating the influence of boundary reflections [26].

The two primary damage indicators utilized in this study were the root mean square deviation (RMSD) of the EMS spectra and the maximum of the fitted envelope of the GW signal. The RMSD was calculated between the baseline and after a certain number of fatigue cycles to evaluate the health of the AUCTs. In case of the EMS measurements, the RMSD was calculated for the entire spectra and the frequency of the first resonance. While, in the case of the GWs, the RMSD was calculated for the maximum of the fitted envelope by Hilbert's transform at two different frequencies namely 50 kHz and 250 kHz.

3. Results and discussion

3.1. Process study and transducer bonding

The temperature profiles corresponding to each combination of process parameters are shown in Fig. 4(a). The process window are all the values enclosed in red color. It is evident that this process window is rather limited. Only specific combinations of process parameters generate the required temperatures for proper melting of the TPAFs. Temperatures resulting from other combinations of process parameters are either inadequate, leading to partial melting of the TPAF or too high, potentially causing thermal degradation to both the AUCT and/or the host structure. This is illustrated in Fig. 4(b) in which three different cases of low, adequate and high generated temperature profiles have been compared to illustrate the significant effects of parameter variation. These findings suggest a delicate balance between process parameters and temperature generated, where deviations can result in detrimental effects on the integrity of the material. It is important to mention here that the temperatures generated are also space-dependent i.e., using the same set of process parameters will result in different temperatures at different locations on the coupon. This spatial heterogeneity could be a critical factor influencing the uniformity of the melting process and, subsequently, the quality of the bond.

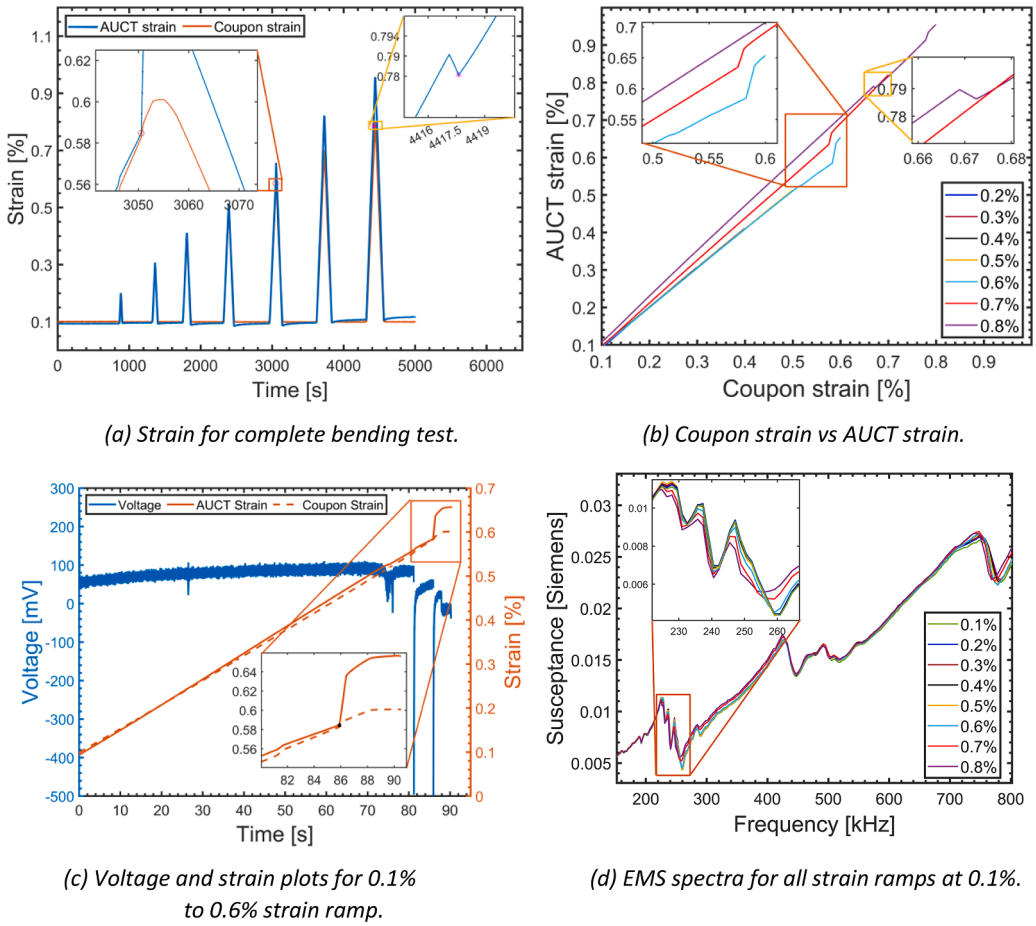

(a) Strain for complete bending test.

(b) Coupon strain vs AUCT strain.

(c) Voltage and strain plots for 0.1% to 0.6% strain ramp.

(d) EMS spectra for all strain ramps at 0.1%.

Fig. 11. AUCT bonded with TPF3 with controlled heating and cooling ramps.

After establishing the process window, the AUCTs were bonded using IH. The bonding process was completed within 1–2 min, demonstrating significantly faster bonding compared to epoxy adhesives or TPAFs melted in an oven. Fig. 5, presents a comparative EMS spectra analysis of AUCTs bonded with TPF3 and TPF4 which were processed in an oven and through IH as well as that of a free AUCT. It can be observed that the EMS spectra of the oven-bonded AUCT and the AUCT bonded using IH using TPF3 are nearly identical and with TPF4 closely resemble each other. This demonstrates that the AUCTs processed with IH are well bonded. However, it is important to note that this resemblance in the EMS spectra was not consistently observed for all TPAFs. For instance, in the case of TPF1, notable variations were noticed between the EMS spectra of AUCTs bonded in the oven and those bonded using IH. The exact cause of this disparity is not fully understood, but it could be attributed to the different heating and cooling ramps experienced by the TPAFs in the oven versus IH. This different processing can influence bond properties and subsequently impact EMS spectra, given that it depends on the bond stiffness of the bond [27]. Nevertheless, analyzing the shift in the resonance frequencies and amplitudes in comparison to a free AUCT, it can be concluded that the AUCTs are well bonded. This suggests that the IH method can produce bonds with comparable mechanical integrity to those formed in an oven, with significantly faster processing times.

3.2. Sensitivity analysis and process control

From the sensitivity analysis, it is observed that both power and time positively affects the generated temperature, whereas C_d has a negative influence on the temperature produced as shown in Fig. 6. Among these factors, power exhibits the most significant influence, followed by C_d and time. An increase in power by 20% correlates with a 67.8% increase in temperature. Whereas, a 20% increase in time and a 20% decrease in C_d yield temperature increments of 16.9% and 20.40%, respectively. A similar pattern is observed when power and time are reduced by 20%, and C_d is increased by 20%. It was also observed that regardless of the duration the induction field is applied, the temperature stabilizes around a certain value for any given combination of power and C_d. This analysis was performed at the center of the coupon. Nevertheless, choosing a different location results in different temperature yet a similar sensitivity pattern is observed. Therefore, it can be concluded that power is the dominant factor in temperature generation while C_d and time show significant effects as well. These results and observations provide valuable insights to have a better temperature control during the induction

Table 5
Critical strains for AUCTs bonded with different TPAFs with different process conditions.

IH bonding method	Adhesive	Material	Mean critical strain [%]	Standard deviation critical strain
Uncontrolled	TPF3	CF-woven PEEK HTA-40	0.56	0.065
	TPF4		0.38	0.008
	TPF5		0.33	0.039
Controlled	TPF3		0.59	0.02
	TPF4		0.57	0.096
	TPF5		0.51	0.03
None	TPF3	CF-unidirectional PEEK APC2-AS4	0.71	0.04
	Reference epoxy adhesive		0.64	0.06

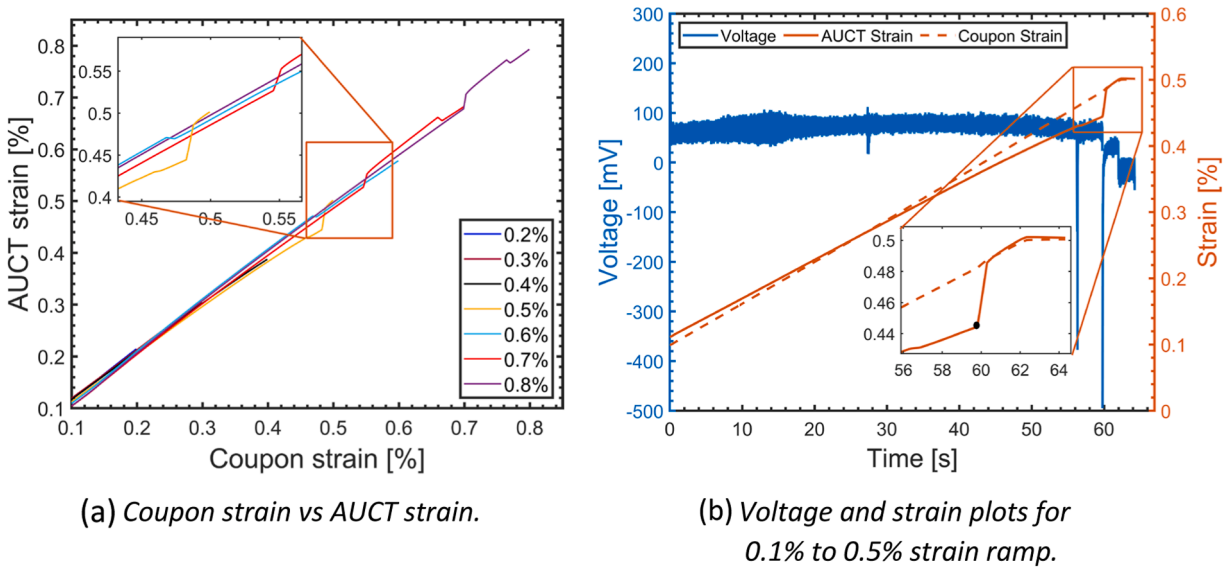

(a) *Coupon strain vs AUCT strain.* (b) *Voltage and strain plots for 0.1% to 0.5% strain ramp.*

Fig. 12. AUCT bonded with TPF3 with uncontrolled heating and cooling ramps.

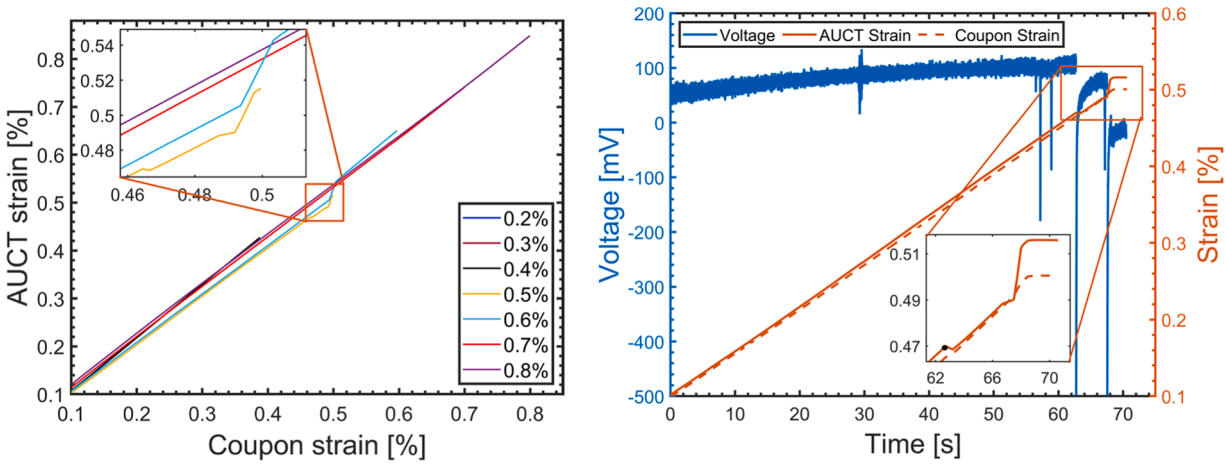

(a) *Coupon strain vs AUCT strain.* (b) *Voltage and strain plots for 0.1% to 0.5% strain ramp.*

Fig. 13. AUCT bonded with TPF5 with controlled heating and cooling ramps.

cycle by dynamically adjusting the power and/or C_d while the process is in progress. This can be achieved by rapidly heating the TPAF to its T_m, maintaining it at that temperature for a desired duration, and then gradually cooling it to its T_g. These findings are presented in Fig. 7. In the first method (shown in solid red line), a power of 150 Amp, C_d of 7 mm, and a time of 35 seconds were utilized. This configuration results in a very high HR (200°C/min), quickly reaching the required temperature of 150°C. The T_m is achieved before the process concludes, and the material is allowed to cool at room temperature, leading to a very high CR (43°C/min). In the second method (shown in solid green), a predefined combination of power (70 Amp) and Cd (3 mm) was employed, leading to a low HR and ensuring the temperature stabilizes around the T_m of the TPAF i.e., 150°C. The T_m is maintained for a desired amount of time (approximately 2-3 minutes) before ending the process. Subsequently, the material is allowed to cool at room temperature, resulting in a rapid cooling, similar to the first method. In this scenario, the time taken to attain the T_m increases significantly by around eight minutes compared to the first case, leading to an inefficient process. In both of these cases, the CR remains high, potentially impacting crystallinity and consequently affecting the mechanical properties of the adhesive bond. In the third method (shown in solid blue line), a power of 150 Amp and a Cd of 3 mm are initially applied to rapidly reach the T_m of the TPAF. Following this, the power is adjusted to 130 Amp, stabilizing the temperature around the T_m (i.e., 150°C) for a few minutes to ensure thorough melting of the TPAF. Subsequently, the power is gradually reduced in incremental steps, leading to a slow cooling of the material until it reaches the T_g of around 45°C. The observed average CR is 12°C/min. The heating and cooling rates achieved during the different processing methods can have a significant influence on the crystallinity and mechanical properties of the TPAF. Consequently, enhanced control of both heating and cooling profiles is essential for optimizing the final adhesive bond. This study indicates that dynamic adjustment of power and/or C_d during the induction process can enhance temperature control, thereby allowing for more effective control of the heating and cooling ramps. Both power and distance were utilized as controlling parameters to govern the heating and cooling ramps. However, for the matter of

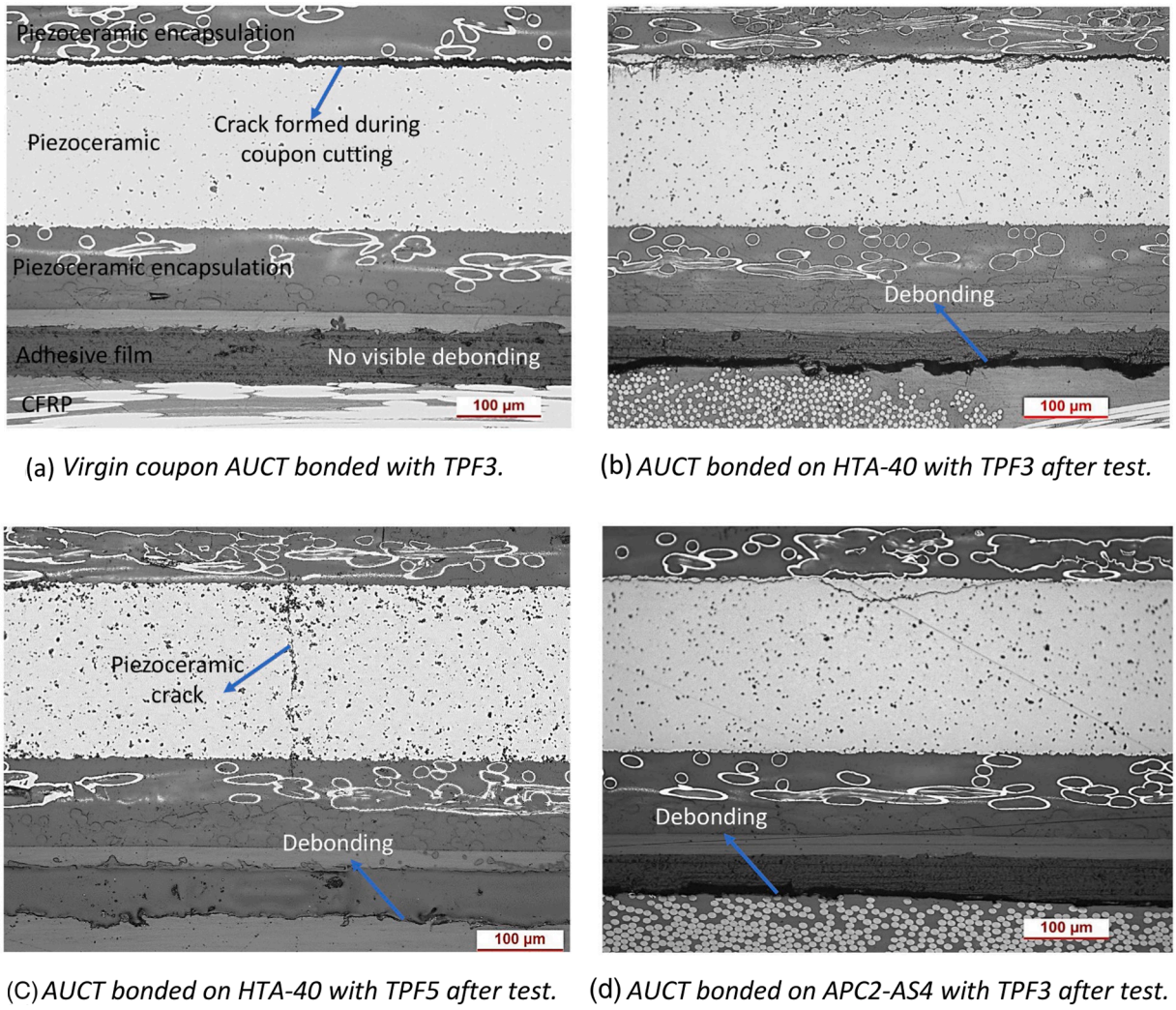

Fig. 14. Micrographs before and after the bending test for AUCTs bonded on different materials with different TPAFs.

discussion, the focus is placed on the power as a controlling parameter. These different processing methods influence the properties of the TPAFs, which are discussed in section 3.4.1.

3.3. Thermal analysis

The results obtained from the investigation of five distinct test cases with different HRs and CRs shown in Fig. 8, simulating three processing methods for the TPF4 and TPF5 are depicted in Figs. 9 and 10 respectively. Fig. 9(a) shows the DSC plots, while Fig. 9(b) shows the values of the T_ms and melting enthalpies obtained during the five distinct test cases for the TPF4. In the case of the TPF4, no considerable variation in the T_m was observed across the five cases. The highest T_m values were observed for cases 1B and 3B, in which isothermal conditions were maintained at the T_m to ensure complete melting of the TPAFs. Conversely, the lowest T_m was observed in the case 1A in which the TPAFs underwent rapid heating and slow cooling. Although there is not a major difference which suggests that the HR and CR do not exert a significant influence on the melting characteristics of the semi-crystalline TPAFs. Analyzing the enthalpy of fusion (melting enthalpy) values, which is a direct indicator of the crystallinity, reveals that cases 3A and 3B which involved slow cooling exhibit the highest crystallinity. The crystallinity itself was not calculated because the theoretical melting enthalpies with 100% crystallinity was not available for the polymers constituting the TPAFs. Thus, it is evident that slow cooling contributes to enhanced crystallinity and, consequently, improved mechanical properties of the adhesive bond. The difference between the melting enthalpy of cases 1B and 3B is not substantial (3.4 J/g), it is crucial to note that processing time for case 3B are 8-10 minutes longer than the case 1B. Therefore, a careful consideration is needed to determine whether the effort justifies the benefits. If the priority is on enhancing the mechanical properties of the adhesive bond, cases 3A or 3B may be preferable for TPAF processing. Conversely, if the focus is on processing efficiency without significant compromise in the mechanical properties, case 1B stands out as a viable option for TPAF processing. Fig. 10(a) and Fig. 10(b) displays the DSC curves and T_gs obtained for the five test cases of TPF5 respectively. For TPF5, characterized by an amorphous structure, the absence of a T_m is noted, and instead, it exhibits a T_g. The results demonstrate almost same T_g values across all five test cases. Therefore, it can be said that the HR and CR do not have a significant influence on the properties of the amorphous TPAF (TPF5).

3.4. Mechanical performance

3.4.1. Static tests

As discussed in Section 2.5, the CS of the AUCTs bonded with three different TPAFs using IH was obtained through a four-point quasi static flexural test. Two different CF reinforcement types were used and AUCTs were bonded with controlled and uncontrolled heating and cooling ramps. The discussion will specifically focus on the AUCTs bonded on

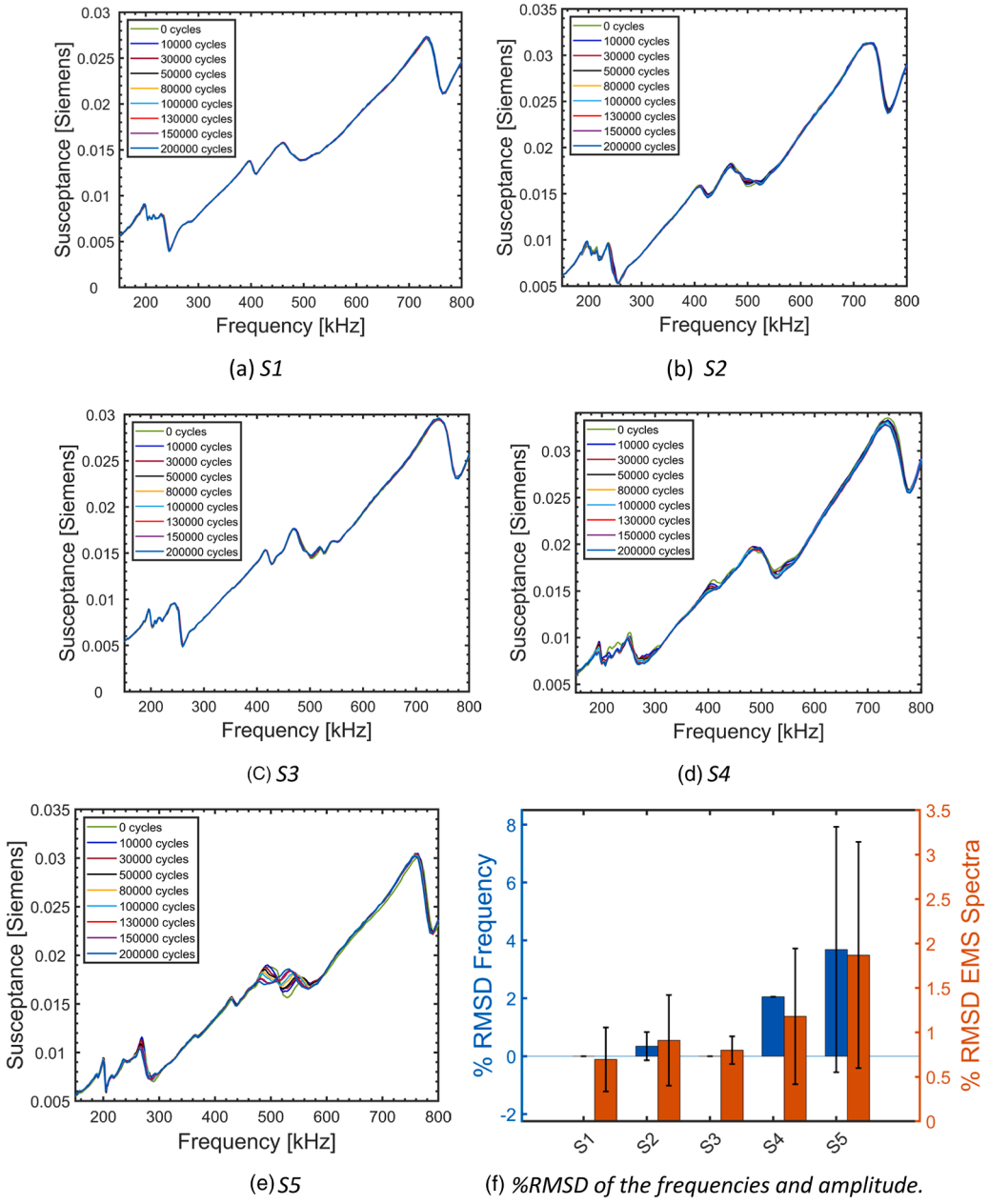

Fig. 15. Fatigue tests (a-e) EMS spectra for the five AUCTs at different fatigue cycles and (f) %RMSD in their respective frequencies and amplitudes for first resonance between baseline and at the end of the test.

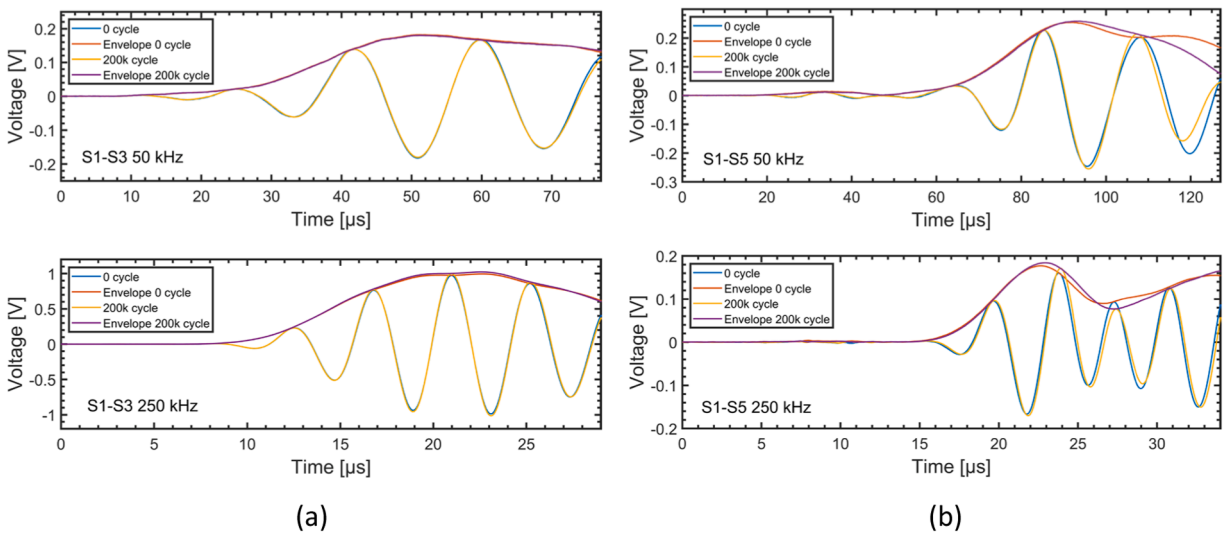

Fig. 16. GWs for different sensor paths at baseline and after the end of the fatigue test. (a) S1-S3 and (b) S1-S5.

Table 6
The %RMSD in the GWs for different sensor paths before and after the fatigue tests.

Sensor path	Mean %RMSD for the maximum of the GW envelope amplitude between baseline and at the end of the fatigue tests.	
	50 kHz	250 kHz
S3-S1	4.84	4.67
S4-S2	7.88	6.40
S1-S3	6.96	3.66
S1-S4	27.25	9.78
S1-S5	14.49	33.46

HTA-40 with a semi-crystalline and the amorphous TPAFs namely TPF3 and TPF5 respectively. For TPF3 both controlled and uncontrolled cases will be discussed, while as for TPF5 only controlled case will be discussed. Similar, approach was used for the others TPAFs bonded on two different CF reinforcements with uncontrolled and controlled heating and cooling ramps to obtain the CS.

3.4.1.1. Controlled case. In this scenario, the heating and cooling ramps were controlled during the IH bonding process of the AUCTs, according to the third method described in the Section 2.3. For the purpose of this discussion, we will focus on one coupon on which the AUCT was bonded with the TPF3. Similar analyses were conducted for various coupons, both for the other samples of this particular TPAF and others. The strain recorded on both the coupon and the AUCT throughout the complete bending test of the coupon under consideration is plotted in Fig. 11(a). When examining the strain measurements, two distinct observations emerge: First, there is a noticeable abrupt rise in the AUCT strain slope, while the strain slope on the coupon may or may not exhibit a significant alteration (shown by red dots). Second, there is an abrupt decline in the AUCT strain slope (shown by magenta stars), however, the strain slope on the coupon remains relatively unchanged. When the crack on the AUCT occurs beneath the strain gauge placed on the AUCT, the strain gauge experiences a sudden increase in the tensile strain and the slope of the tensile strain. This abrupt elevation in the AUCT strain slope is speculated to be associated with this particular crack type. Conversely, when the crack on the AUCT occurs outside the strain gauge placed on the AUCT, the strain gauge experiences a relatively compressive strain despite the overall strain on the AUCT being tensile, this results in a sudden decrease in the strain and the slope of tensile strain. Similar effects arise in scenarios involving debonding between the AUCT and the host surface, leading to a strain relaxation and decline in the tensile strain slope. Therefore, the distinction between the location of the crack relative to the gauge influences whether the strain slope change is perceived as tensile or compressive. These abrupt changes in the strain serve as a valuable indicator for assessing the health of the AUCT. Both of these fluctuations are accompanied by spikes in the voltage signal.

Fig. 11(b) shows a plot of strain recorded on the coupon against the strain observed on the AUCT for each strain ramp. Up to the 0.5% strain ramp, a nearly linear correlation is evident, indicating close similarity in strain between the coupon and the AUCT, without any noticeable fluctuations until the AUCT break. This indicates a consistent load-sharing behavior and strong adhesive integrity, as strain is uniformly transferred without fluctuations. However, for the 0.6% and 0.7% strain ramps, a sudden increase in AUCT strain is observed which corresponds to a crack occurring beneath the strain gauge on the AUCT. Additionally, the fluctuation in the slope of the AUCT strain during the 0.8%, corresponds to a crack occurring outside the strain gauge on the AUCT, or debonding between the AUCT and the composite surface. Fig. 11(c) shows a time plot featuring multiple y-axes that depict voltage measured on the AUCT and strain values for the coupon and the AUCT during a strain ramp of 0.1% to 0.6% on the coupon under discussion. This particular ramp was selected because it was the initial strain ramp where a spike in both strain and voltage signals was detected, as indicated in Fig. 11(a) and (b). As the strain increases from 0.1% to 0.6%, the voltage response remains relatively steady until the AUCT breakage, is marked by a sudden spike in the voltage signal. This spike in voltage is a result of the piezoelectric effect triggered by an abrupt change in the strain experienced by the AUCT. To determine the CS, the strain for this ramp is plotted together with the voltage signal as shown in Fig. 11(c). The strain on the coupon where this first voltage spike is accompanied with a decrease in the voltage signal is considered as the CS. The CS is encircled in magenta in Fig. 11(a) and highlighted by a black dot in Fig. 11(c). This effect, where sudden changes in the strain and voltage occur, marks the critical point of AUCT failure and indicates the fracture point and hence the CS of the AUCT. A few fluctuations in the strain data are also observed at some points of the voltage signal which are caused due to the machine and not attributed to any changes in the AUCT characteristics, as also confirmed by corresponding strain values. The breaking of the AUCT was clearly audible during the test.

The EMS spectra measured at 0.1% strain following each loading and unloading strain ramps are shown in Fig. 11(d). An observable shift in the EMS spectra occurs notably after the application of 0.6% strain, consistent with earlier findings obtained from the voltage and strain data. This shift suggests an onset of damage within the AUCT or debonding from the host surface, which manifests as detectable

alterations in the EMS response. Following the 0.6% strain, reductions are observed in both the frequency and the amplitude of the first resonance, which continue to diminish further during the 0.7% and 0.8% strain ramps. These continuous reductions in resonance parameters beyond 0.6% strain imply progressive material degradation, likely associated with cumulative cracking or debonding effects. From these analyses the average CS for all coupons for this TPAF bonded under controlled conditions was found to be 0.59% as shown in Table 5. This CS value provides a quantifiable threshold for assessing AUCT's health and bond integrity.

3.4.1.2. Uncontrolled case. This section discusses the results for an AUCT bonded on a HTA-40 coupon with TPF3 under uncontrolled cooling ramps. This allows for comparison with the controlled conditions of the same TPAF, which is helpful for understanding how temperature control can influence the bond properties. The CS was determined following the same methodology as that of uncontrolled case discussed previously. Similar trends were observed in the controlled case, characterized by sudden fluctuations in the strain data during specific strain ramps. Specifically, in this case, the initial fluctuation is observed during the 0.5% strain ramp. The strain recorded on the coupon vs the strain measured on the AUCT for each strain ramp is shown in Fig. 12(a). A sudden increase in AUCT strain is observed during the 0.5% strain ramp. Additionally, a sudden decrease in the strain was observed during the 0.6% strain ramp, and for the 0.7% and 0.8% strain ramp, both sudden increase and decrease in the strain were observed. The coupon strain, the AUCT strain, and the corresponding voltage measured on the AUCT are plotted for the strain ramp of 0.1% to 0.5% in Fig. 12(b). In the case of uncontrolled cooling ramps, small deviations between the AUCT and coupon strain are observed even before AUCT damage, a behavior absent in the controlled cooling scenario. These findings reinforce the idea that controlled cooling ramps stabilize strain behavior, as uncontrolled conditions result in early strain fluctuations prior to cracking and an increase in overall strain variability. The average CS for all coupons of TPF3 was found to be 0.56% as shown in Table 5.

In Fig. 13(a) and Fig. 13(b), similar plots are presented for the amorphous TPAF namely TPF5. While examining TPF3, it was noticed that the strains on the coupon and the AUCT were quite similar until the breakpoint. However, in the case of TPF5, the AUCT showed higher strains than the coupon even before reaching the breakpoint. Moreover, the slope of the voltage curve for TPF5 was notably steeper compared to TPF3 in both controlled and uncontrolled cases. This disparity is attributed to higher Shear modulus of the TPF5 (2.81±0.11 MPa as compared to 1.52±0.31 MPa for TPF3), resulting in increased strain transmission from the coupon to the AUCT, consequently leading to a steeper voltage curve slope. This characteristic is advantageous in the transmission and reception of GWs. However, it also can cause the AUCT to fail at lower strains, as can be seen in Table 5 that TPF5 exhibits lower CS values for both controlled and uncontrolled cases as compared to TPF3 which has comparatively lower Shear modulus. The CS of all the AUCTs bonded with controlled and uncontrolled on different materials with various TPFs is shown in Table 5.

It can be seen that the AUCTs bonded with a controlled induction cycle have higher CS. This is expected as slower cooling can increase the crystallinity and therefore the mechanical properties. However, the induction time also increases around by a factor of 10 (from 1–2 min to 10–11 min). Based on the application if higher CS is desired then the controlled induction ramp can be used, otherwise, if the required CS strain is lower, then the uncontrolled induction ramp can be applied. The average CS of the AUCTs bonded with TPF3 on the APC2-AS4 coupons through controlled IH ramps was found to be 0.71%, exceeding the controlled case of AUCTs bonded with TPF3 on the HTA-40 material by more than 0.1%. This higher CS in the APC2-AS4 composite can be attributed to two primary factors. Firstly, the higher surface roughness of the APC2-AS4 material may contribute to improved bonding. Secondly, the unidirectional nature of APC2-AS4, characterized by a continuous surface and consistent fiber alignment, facilitates enhanced contact and creates more uniform bonding. For reference, previous studies have reported the CS for similar AUCTs which were either co-bonded or bonded with epoxy adhesives on the composite coupons to be 0.58% [20], 0.5% [21], and 0.58% [28]. The average CS of AUCTs bonded with the reference epoxy film in this study was 0.64%. Therefore, it can be inferred that the AUCTs bonded using the proposed method with TPAFs exhibit comparable if not superior, mechanical performance in terms of the ultimate strain.

The micrographs of certain coupons before and after undergoing the bending tests are shown in Fig. 14(a-d). These images reveal various failure modes, including debonding between the AUCT and the adhesive, debonding between the composite and the adhesive, and cracks within the AUCT. Notably, there is an absence of delamination in the AUCT, which itself is a composite composed of an encapsulation layer, electrode layer (Copper mesh), and the piezoceramic, indicating a robust transducer structure. The separation occurs predominantly at the interface between the composite and the adhesive, rather than at the interface between the AUCT and the adhesive as observed in most of the micrographs. This indicates that the bonding affinity at the composite and adhesive interface is weaker compared to the AUCT and adhesive interface. This could be because PEEK is a high-performance polymer with low surface energy and does not bond easily. This insight underlines the necessity of surface treatments or alternative adhesives to enhance bond strength with PEEK substrates. Additionally, a delamination and/or crack running along the length of the AUCT is visible on the upper side of the piezoceramic in both tested and untested cases. Since this crack or delamination is also present in the untested case, it is suspected to have formed during the cutting and polishing process of the coupon rather than during the bending tests.

3.4.2. Cyclic tests. The preliminary assessment of the long-term performance of the AUCTs bonded with different TPAFs (S1-S5) was carried out through tensile-tensile fatigue tests. However, this evaluation represents only an initial study, and further in-depth research is needed to draw conclusive results. The EMS spectra of different AUCTs measured at the baseline and after a specified number of fatigue cycles are shown in Fig. 15(a-e). The results show a minimal change in the EMS spectra of the AUCTs S1, S2, and S3, suggesting good fatigue resistance and structural integrity, particularly for S1 and S3. However, a notable change was observed in the EMS spectra of the S4 and S5. This was observed in both of the two coupons tested. The change in EMS was analyzed across two parameters: the RMSD in the entire EMS spectrum and the frequency of the first resonance. The mean %RMSD change between the baseline (first measurement) and the post-test frequencies and amplitudes for the first resonance for S1 to S5 is plotted in Fig. 15(f). A minor change in the EMS spectra was observed across all the AUCTs, with the biggest mean RMSD of 1.9% occurring in case of S5, followed by S4 with a deviation of 1.2%. Regarding the change in the first resonance frequency, no change was observed in the case of S1 and S2, whereas in the other AUCTs, a minor change in the frequencies was observed. The biggest change occurred in S5 with a total mean RMSD of 3.7%, followed by S4 with a mean change of 2.1%. Hence, S1 and S3 demonstrated exceptional performance, with minimal changes observed in both the EMS spectrum and the resonant frequency, indicating minimal AUCT damage or debonding. Conversely, in the case of S4 and S5, some changes were observed, although they were not significant, indicating moderate durability in cyclic loading.

In addition to examining the EMS spectra, GW signal measurements served as an additional indicator for assessing the performance of the AUCT in the fatigue tests and offer a more comprehensive understanding of AUCT behavior under cyclic loading. For the sake of the discussion, two cases are presented showing results for S3 and S5, which represent

minor to significant change in the EMS spectra as shown in the previous section. Fig. 16(a) depicts GWs actuated at S1 and received at S3 at 50 KHz and 250 kHz, with a fitted envelope using the Hilbert transform, both at baseline and after the completion of the fatigue test for the initial segment of the signal. Similarly, Fig. 16(b) shows the same for the sensor path S1-S5. The comparison reveals a minor change in the amplitude of the GWs after the fatigue test for the S1-S3 sensor path with a mean RMSD of less than 10%. However, in the case of the sensor path S1-S5, some significant changes are observed in the amplitude of the wave with a mean RMSD of 33.4%, alongside an observable shift in the 250 kHz frequency wave. These findings align with the observations made in the EMS results. Specifically, the AUCT S3 showed minor changes in its EMS spectra, thereby reflecting minor alterations in the GW signals. Conversely, AUCT S5 exhibited significant changes in the EMS spectra, which were also observable in the GWs. These observations underline the utility of combining EMS spectra and GW measurements as more comprehensive measurements for assessing AUCT performance in fatigue tests, allowing for more informed diagnosis of AUCTs in practical applications. The RMSD in the GW amplitude for different sensor paths is presented in Table 6. It is important to note that only two coupons were tested in the fatigue assessment, and the relatively high standard deviation observed in the results indicates that additional testing is necessary to draw definitive conclusions. Conducting a larger number of tests will provide a more robust statistical analysis, allowing for a clearer understanding of the performance variability across different TPAFs.

4. Conclusion

A novel, rapid, and economical method of bonding PZTs to composites using IH is proposed in this study. The study demonstrated a significant reduction in bonding time from hours to minutes for attaching AUCTs to composite parts using TPAFS. Therefore, significantly enhancing the process efficiency. An extensive study was carried out to understand the fundamentals of the process and examine the influence of different process parameters. The main findings are summarized below:

Process insights:

- Among the process parameters, power has the highest influence on the temperatures generated.
- Dynamic adjustments of power and/or C_d enable controlled heating/cooling ramps to process semi-crystalline TPAFs for bonding the PCTs.

Material findings:

- Semi-crystalline TPAFs showed minor crystallinity increases; the T_g of the amorphous TPAF did not show significant change.
- PCTs bonded with semi-crystalline as well as the amorphous TPAF exhibited good CS, with some outperforming conventional epoxy-bonded or oven-bonded counterparts.
- Fatigue performance was excellent for TPF1-TPF3; TPF4 and TPF5 showed significant changes during the fatigue test.

Conclusions:

- The proposed novel method is an efficient bonding procedure for PCTs to composite structures, demonstrating its rapidity, cost-effectiveness, and capability for industrial bonding.
- Processing of TPAFs does not adversely affect their properties.
- PCTs bonded with some TPFs particularly TPF3, demonstrated the capability to endure high strains and exhibited good performance under sustained loads over extended durations.

In this study, only two fatigue tests were conducted, which is insufficient to draw definitive conclusions regarding the long-term performance of AUCTs bonded with the proposed TPAFs. Therefore, further testing is necessary to determine the performance of the AUCTs bonded with the proposed TPAFs over extended fatigue tests and cycles. Additionally, it is essential to assess the potential of this proposed technique in terms of signal quality and accurate damage detection when compared to a conventional bonding method.

Hence, expanding upon this study would involve performing additional fatigue testing with an increased number of fatigue cycles as well as additional environmental condition assessments. Moreover, the aim would involve measuring the signal quality acquired from the AUCTs bonded through the proposed approach and evaluating their efficiency in accurately detecting damage within composite structures. Exploring the potential extension of this method to attach other sensors like strain gauges, fiber Bragg grating sensors, etc., presents an intriguing topic for investigation. Additionally, investigating the feasibility of an automated bonding process for PCTs onto composite structures using this inventive method would be an exciting area for further exploration.

Declaration of generative AI and AI-assisted technologies in the writing process

During the preparation of this work the author used ChatGPT in order to improve language. After using this tool, the author reviewed and edited the content as needed and take full responsibility for the content of the publication.

Funding

This paper is part of the ENHAnCE ITN project (https://h2020-enhanceitn.eu/), (accessed on 01 March 2024) funded by the European Union's Horizon 2020 research and innovation programme under the Marie Skłodowska-Curie grant agreement No. 859957.

CRediT authorship contribution statement

Tasdeeq Sofi: Writing – original draft, Software, Methodology, Investigation, Formal analysis, Data curation, Conceptualization. **Javier A. García:** Writing – review & editing, Resources, Investigation. **María R. Gude:** Writing – review & editing, Supervision, Methodology, Investigation. **Peter Wierach:** Writing – review & editing, Supervision.

Declaration of competing interest

The authors declare that they have no known competing financial interests or personal relationships that could have appeared to influence the work reported in this paper.

Acknowledgements

The authors would like to thank Rafael Contento from FIDAMC and Dr.-Ing. Till Julian Adam from D.L.R for help with carrying out the experimental investigation.

Data availability

Data will be made available on request.

References

[1] V. Giurgiutiu, Chapter 1 - Introduction, in: V. Giurgiutiu (Ed.), Structural Health Monitoring of Aerospace Composites, Academic Press, Oxford, 2016, pp. 1–23, https://doi.org/10.1016/B978-0-12-409605-9.00001-5. URL, https://www.sciencedirect.com/science/article/pii/B9780124096059000015.

[2] A. Güemes, A. Fernandez-Lopez, A.R. Pozo, J. Sierra-Pérez, Structural health monitoring for advanced composite structures: a review, J. Compos. Sci. 4 (2020) 13, https://doi.org/10.3390/jcs4010013.

[3] X. Qing, W. Li, Y. Wang, H. Sun, Piezoelectric transducer-based structural health monitoring for aircraft applications, Sensors 19 (2019), https://doi.org/10.3390/s19030545.

[4] F. Lambinet, Z.Sharif Khodaei, Development of hybrid piezoelectric-fibre optic composite patch repair solutions, Sensors 21 (2021), https://doi.org/10.3390/s21155131.

[5] D.P. Roach, S. Neidigk, Does the maturity of structural health monitoring technology match user readiness?. 8th International Workshop on Structural Health Monitoring, 2011. Stanford, CA, USAURL, https://www.nasampe.org/store/viewproduct.aspx?id=4373826.

[6] C. Tuloup, W. Harizi, Z. Aboura, Y. Meyer, K. Kamel, R. Lachat, On the manufacturing, integration, and wiring techniques of in situ piezoelectric devices for the manufacturing and structural health monitoring of polymer–matrix composites: a literature review, J. Intell. Mater. Syst. Struct. 30 (2019) 2351–2381, https://doi.org/10.1177/1045389X19861782.

[7] D.Sáenz del Castillo Gutiérrez, Characterization and Real-Time Process Monitoring of Thermoplastic Composites Manufacturing processes, Ph.D. Thesis, Universidad Politécnica de Madrid, 2020. URL, https://dialnet.unirioja.es/servlet/dctes?codigo=291911.

[8] T. Sofi, M.R. Gude, P. Wierach, I. Martin, E. Lorenzo, An efficient procedure for bonding piezoelectric transducers to thermoplastic composite structures for SHM application and its durability in aeronautical environmental conditions, Sensors 23 (2023), https://doi.org/10.3390/s23104784.

[9] T.J. Ahmed, D. Stavrov, H.E.N. Bersee, A. Beukers, Induction welding of thermoplastic composites—an overview, Compos. - A: Appl. Sci. Manuf. 37 (2006) 1638–1651, https://doi.org/10.1016/j.compositesa.2005.10.009.

[10] T. Bayerl, M. Duhovic, P. Mitschang, D. Bhattacharyya, The heating of polymer composites by electromagnetic induction – a review, Compos. - A: Appl. Sci. Manuf. 57 (2014) 27–40, https://doi.org/10.1016/j.compositesa.2013.10.024.

[11] M. Dhondt, Induction Welding of High Performance Thermoplastic composites, Master's thesis, Delft University of Technology, Delft, 2020. URL, https://repository.tudelft.nl/islandora/object/uuid%3Ae8dfe899-de2d-4d84-8300-132ce5154c89.

[12] J.W. van Ingen, A. Buitenhuis, M. van Wijngaarden, F. Simmons III, Development of the Gulfstream G650 induction welded thermoplastic elevators and rudder, in: International SAMPE Symposium and Exhibition, Seattle, WA, USA, 2010.

[13] B. Sosnowchik, R. Azevedo, D. Myers, M. Chan, A. Pisano, L. Lin, Rapid silicon-to-steel bonding by induction heating for MEMS strain sensors, J. Microelectromechanical Syst. 21 (2012) 497–506, https://doi.org/10.1109/JMEMS.2011.2179013.

[14] M. Wang, Y. Mei, W. Hu, X. Li, G.-Q. Lu, Pressureless sintered-silver as die attachment for bonding Si and SiC chips on silver, gold, copper, and nickel metallization for power electronics packaging: the practice and science, IEEE J. Emerg. Sel. Top. Power Electron. 10 (2022) 2645–2655, https://doi.org/10.1109/JESTPE.2022.3150223.

[15] P. Rochala, C. Hofmann, M. Kroll, S. Panhale, R. Javed, K. Hiller, Inductive sintering of silver micro particles for bonding of microelectronic components, Electronics 12 (2023), https://doi.org/10.3390/electronics12153247.

[16] L. Qiwei, P.Robert James, Y. Fan, K.W. Flanagan, J.N. Barshinger, W. Lin, I. Dris, Methods For Bonding High Temperature Sensors, 2009. URL, https://patentimages.storage.googleapis.com/66/7a/74/0ca5d59d664924/US20090110845A1.pdf.

[17] N. Yue, S.Z. Khodaei, M.H. Aliabadi, An innovative secondary bonding of sensors to composite structures for SHM application, in: advances in fracture and damage mechanics XVII, Key Eng. Mater. 774 (2018) 516–522, https://doi.org/10.4028/www.scientific.net/KEM.774.516.

[18] P. Wierach, Electromechanical Functional Module and Associated Process, 2005. URL, https://worldwide.espacenet.com/publicationDetails/originalDocument?FT=D&date=20070925&DB=&locale=en_EP&CC=US&NR=7274132B2&KC=B2&ND=6.

[19] Y. Furushima, C. Schick, A. Toda, Crystallization, recrystallization, and melting of polymer crystals on heating and cooling examined with fast scanning calorimetry, Polym. Cryst. 1 (2018) e10005, https://doi.org/10.1002/pcr2.10005.

[20] M. Moix-Bonet, I. Buethe, M. Bach, C.-P. Fritzen, P. Wierach, Durability of co-bonded piezoelectric transducers, Proc. Technol. 15 (2014) 638–647, https://doi.org/10.1016/j.protcy.2014.09.025.

[21] I. Mueller, C.-P. Fritzen, Inspection of piezoceramic transducers used for structural health monitoring, Materials 10 (2017) 71, https://doi.org/10.3390/ma10010071.

[22] G. Park, C.R. Farrar, F.L. di Scalea, S. Coccia, Performance assessment and validation of piezoelectric active-sensors in structural health monitoring, Smart Mater. Struct. 15 (2006) 1673, https://doi.org/10.1088/0964-1726/15/6/020.

[23] T. Feng, D. Bekas, M.H.F. Aliabadi, Active health monitoring of thick composite structures by embedded and surface-mounted piezo diagnostic layer, Sensors 20 (2020) 3410, https://doi.org/10.3390/s20123410.

[24] D.G. Bekas, Z. Sharif-Khodaei, M.H.F. Aliabadi, An innovative diagnostic film for structural health monitoring of metallic and composite structures, Sensors 18 (2018) 2084, https://doi.org/10.3390/s18072084.

[25] T. Feng, M.H.F. Aliabadi, Structural integrity assessment of composites plates with embedded PZT transducers for structural health monitoring, Materials 14 (2021), https://doi.org/10.3390/ma14206148.

[26] Z. Sharif Khodaei, M. Aliabadi, Assessment of delay-and-sum algorithms for damage detection in aluminium and composite plates, Smart Mater. Struct. 23 (2014) 075007, https://doi.org/10.1088/0964-1726/23/7/075007.

[27] M.M. Islam, H. Huang, Understanding the effects of adhesive layer on the electromechanical impedance (EMI) of bonded piezoelectric wafer transducer, Smart Mater. Struct. 23 (2014) 125037, https://doi.org/10.1088/0964-1726/23/12/125037.

[28] I. Buethe, M. Moix-Bonet, P. Wierach, C.-P. Fritzen, Check of piezoelectric transducers using the electro-mechanical impedance, in: 7th European Workshop on Structural Health Monitoring, IFFSTTAR, Nantes, France, 2014. URL, https://inria.hal.science/hal-01020432.